Probabilistic Climate Change Projections for South East Australia: Surface Warming Examples

Date: 1 November 2006

Author: Ian G. Watterson

1. Introduction

We wish to provide improved methods of projecting climate change for Australia, building on the previous Climate Impact Group (CIG) approach described by Whetton et al. (2005). The main aim is to provide a confidence weighting throughout the range of change considered plausible, basing this on the data from simulations by a number of current climate models. For most quantities this means, in effect, a 'probability density function' (PDF) for the change variable. Several recent studies have provided such results based on various approaches and assumptions, often of considerable complexity. A new, relatively simple method, extending that of the CIG, was outlined in my previous note (Watterson, 2006). This is applied to a more realistic case here, to produce surface warming projections over south east Australia (specifically, the domain depicted in Figure 1). The models used and a simple estimation of weighting of them is presented in section 2. (I am able to make use of results prepared for both the SEACI and ACCSP modelling projects here.) Patterns of change (scaled by global mean warming) are considered in Section 3, and probabilistic scaled warming is presented, determined using five approaches. The distributions for net warming under three idealised global mean warming distributions are calculated and presented in Section 4.

2. GCM simulations of climate and climate change for South East Australia

In support of the 2007 Fourth Assessment Report on climate change by the IPCC, a major climate simulation project has been organised by the World Climate Research Program. Some 17 modelling centres from 9 countries have performed simulations of the period 1870-2100 and beyond, using their current climate models. The experiments include prescribed greenhouse gas (GHG) and aerosol changes based on observations to 2000, then following one of three SRES scenarios to 2100, with constant forcing thereafter. Data from some 22 models are currently being considered for the new CSIRO projections. This report considers only four individual models, but briefly compares these to the 'multi-model mean' (courtesy Julie Arblaster). The models are listed in Table 1. Preliminary data from the new version of CSIRO's current model 'Mk3.5' are included here. Results from HadGem and GFDL are courtesy of Janice Bathols and Ian Macadam.

Averages for both the full year and the four seasons over the period 1961-1990 have been formed for a number of quantities, including surface air temperature, precipitation and sea-level pressure. These are presented in my upcoming report for SEACI. A simple skill assessment of these quantities is shown in Fig. 2. All four models simulate both the area mean and local values quite well, in comparison to the 0.25° gridded observational data for temperature and precipitation from the Bureau of Meteorology. Data from ERA reanalyses are used as the observational fields for SLP. Interestingly, the multi-model mean compares slightly better than the individual models, except that HadGem just beats it in two quantities. The ERA rainfall field suffers from well-known problems and scores no better than the models. Some bias may exist from using the averages of daily max and min temperatures as the observational field.

Consideration of an appropriate weighting of models is not the topic of this note. Ideally, this could be based on the (hypothetical) ability of models to simulate the local climate change in a particular field, scaled (or normalised) by the global mean warming. For illustration, we consider here the mean of the seasonal averages in Fig. 2, averaged over the three quantities, as a weight. Dividing by the sum of the four results gives the numbers in Table 1. This rather uniform set of weights will be used for all grid points in the example presented shortly.

Table 1. Models considered in the study, the weight assigned to them and the global mean warming to 2100 under A1B.

Model Name	**Origin**	**Weight**	**Warming (K)**
Mark 3.0	CSIRO Atmospheric Research	0.234	2.21
Mark 3.5	CSIRO Atmospheric Research	0.239	3.43
HadGem	UK Meteorological Office	0.273	3.53
GFDL 2.1	Geophys. Fluid. Dyn. Lab., USA	0.254	2.76
MMM	Multi-Model Mean		2.89

In the multi-model means, the ‘Murray Darling Basin’ regional annual mean change in temperature divided by the global mean is between 1.105 and 1.158 for all SRES scenarios and time periods. Thus, there appears to be little systematic bias in using scaled patterns over the region (see also Watterson, 2005).

Changes from 1976 to 2100 have been determined by linear interpolation between the 1961-90 and 2071-2100 averages. Global mean warmings for this span under the A1B scenario from the models are given in Table 1. (Note that there is no account of control model drift in these values, which would boost the Mk3.0 result to one close to the MMM result.) Maps of the scaled change of temperature for summer (DJF), interpolated to a common 1° grid, are shown in Fig. 1.

The individual model results are determined from land points only (1a to 1d). As described by Watterson et al. (2006) simulations at 0.5° by CCAM show that a sharp drop in warming occurs at coasts, on going from land to ocean. It would seem wise to avoid linear interpolation between land and ocean points as a means of producing values

near the real coastline. To assist in producing interpolated values nearer the coast, the model fields are first interpolated to a double grid, using extrapolation to the edges of coastal land squares. The final 1° grid fields are plotted using cell colouring. In fact, the HadGem and (apparently) GFDL models allow squares with fractional surface types. The relatively low values on points that extend beyond the true coast are a result of this. Averaging over the four models (with weights) avoids these values if points with less than four model results are omitted (compare the 1e and 1f maps). A weighted average of results simply interpolated from the full grid is in 1g. The difference over land is rather small in this case, due to the relatively high resolution of the models (2° or better). The simple average over all 22 models, 1h, produces less abrupt land-sea contrast, partly due to differing and often coarser model grids and coastlines.

3. Distributions for scaled change

In the previous note, a number of methods for generating a PDF for scaled change of a certain quantity at a single point were described. These are illustrated in Fig. 3, using data for warming at the central point of the map, 142°E and 31°S. Allowing for statistical uncertainty, the true value for each model (from multiple runs) is assumed to be from a simple normal PDF centred on the sample value. The uncertainty is determined from that appropriate to differences of two 30-y means, assuming these follow from the interannual standard deviation field, then scaled. The available SD field from Mk3.0 is used for all models here, with the result scaled by 3K. The four sample change ratios here are 1.23, 1.42, 1.02 and 1.55. The common uncertainty SD is 0.11. The weighted sum of the four individual distributions is the ‘Sum’ PDF in Fig 1. The normal distribution fitted to this Sum curve is also shown (as Normal). The range of ratio values allowed here extends from the point where the corresponding cumulative distribution (CDF) is 0.001 to the point where it is 0.999. 1000 values are used to provide close representation of all the curves. These will differ for each grid point –there being no need for them to be common here.

The beta distribution fit to the Sum curve is also shown. Here the end points (two of the four parameters) give the 0.01 and 0.99 values of the CDF of Sum. The steep sides of Sum here lead to sharply dropping sides of Beta. The Uniform distribution is between the smallest and largest of the four change ratios. The choice of second smallest and largest (which would be unwise for four values) would match the original CIG approach.

The final curve ‘Narrow’ is a normal fit to Sum, but with the SD reduced by the square root of the ‘effective N’. This is the number of models, with allowance for uneven weighting, being the inverse of the sum of the squared weights. This distribution would be appropriate if one considered the various model results to be a sample from a normal distribution centred on the ‘true’ change. It would represent a plausible distribution for the ‘true’ value, whose uncertainty will be smaller the more models are used, as in standard statistical theory.

A range of statistics from each of these distributions can be determined. The means match that from the original model results -except in the Uniform case. The SDs vary

somewhat, being smallest for Narrow, of course. Percentiles can be readily determined from the CDFs.

Applying the methods to every grid point with four model (land) values produces a map of means that matches 1f (even Uniform is very close). Plotted in Fig. 4 are the 10, 50 and 90 percentiles from all five cases. As anticipated from Fig. 3 the 10 to 90 range is usually smaller for Uniform and Narrow than for the other three.

4. Net warming for 2100

As in the CIG method, the patterns of scaled warming need to be combined with a global mean warming distribution to produce a net change. As described in the previous note, the assumption is made that the scaled local change 'x' and the global warming 'T' are considered two independent variables. The joint distribution function is simply the product of the two PDFs. Statistics of the net local change can be determined numerically from this joint function.

Consider first the trivial case, where one proposes that the global warming has reached a single specific amount. For the A1B scenario in 2100, a value around 3 K is suggested by the models (Table 1). Suppose for simplicity it is exactly 3K. Then the joint PDF for the local warming is only trivially different from the scaled warming PDF, and all the statistics correspond to those from section 3, with a factor of 3 K. For instance, the maps in Fig. 4 apply to the net case, but with the scale amplified to range from 1.2 K to 6 K.

An idealised PDF that better reflects the uncertainty in global warming in this case, which I used previously, is illustrated in Fig. 5 –the SD=1K case. It is necessary to discretise this normal distribution, and 100 T points seem adequate. Now if the local warming ratio is a single value, say 1, the joint distribution is again simple. The net warming distribution is the same of the global result in Fig. 5.

For the more general case additional calculations are needed. Two methods were used previously. One is a straight forward evaluation of the joint function at each x and T step. This gives 100000 values of probability, each corresponding to a net warming P simply given by xT. Ordering these by P allows a simple conversion to a CDF as a function of P. The second method makes use of the simple form for P, and the separate nature of the joint function. This appears to be computationally more efficient by a factor of about 10.

The net warming PDFs for the central point, determined for the SD=1 global warming case and each scaled case, are shown in Fig. 6. The differences are surprisingly small. The Uniform and Narrow cases give a slightly narrower net warming. Performing the calculation at every grid point leads to the maps shown in Fig. 7. Again, there is very little difference across the five for the 10, 50 and 90 percentiles shown.

The similarity across the five cases is due to the scaled warming PDFs being all relatively narrow, in comparison with the global warming one. A case intermediate between the SD=1 case and the single T case above is for the SD = 0.2 curve shown in Fig. 5. This

produces the net warming curves for the central point shown in Fig. 8. The PDFs more closely reflect the differences in Fig. 3.

5. Summary

This note applies the method previously described for generating PDFs for scaled warming and net warming to points over SE Australia. The range of possible results at each point is evident from the maps of 10 and 90 percentile statistics that are generated. The choice of the four models and their weighting used here is only for example purposes.

As previously, five different types of scaled warming PDF are considered. Support for using each of these could be argued, although the uniform distribution, with no weighting of models is clearly outdated. The three other methods of fitting the spread of individual model results produce rather similar net warmings, in practice. The Beta case has the advantage of allowing a non-zero skewness and a finite range using only four parameters. Given the popularity of Bayesian methods, which (as I understand it) lead to narrowing ranges as the number of models increases, the Narrow case should also be considered. Fortunately, evaluation of all five cases, even for multiple T scenarios, seems quite feasible. Application of the method to a larger set of models and other variables is recommended.

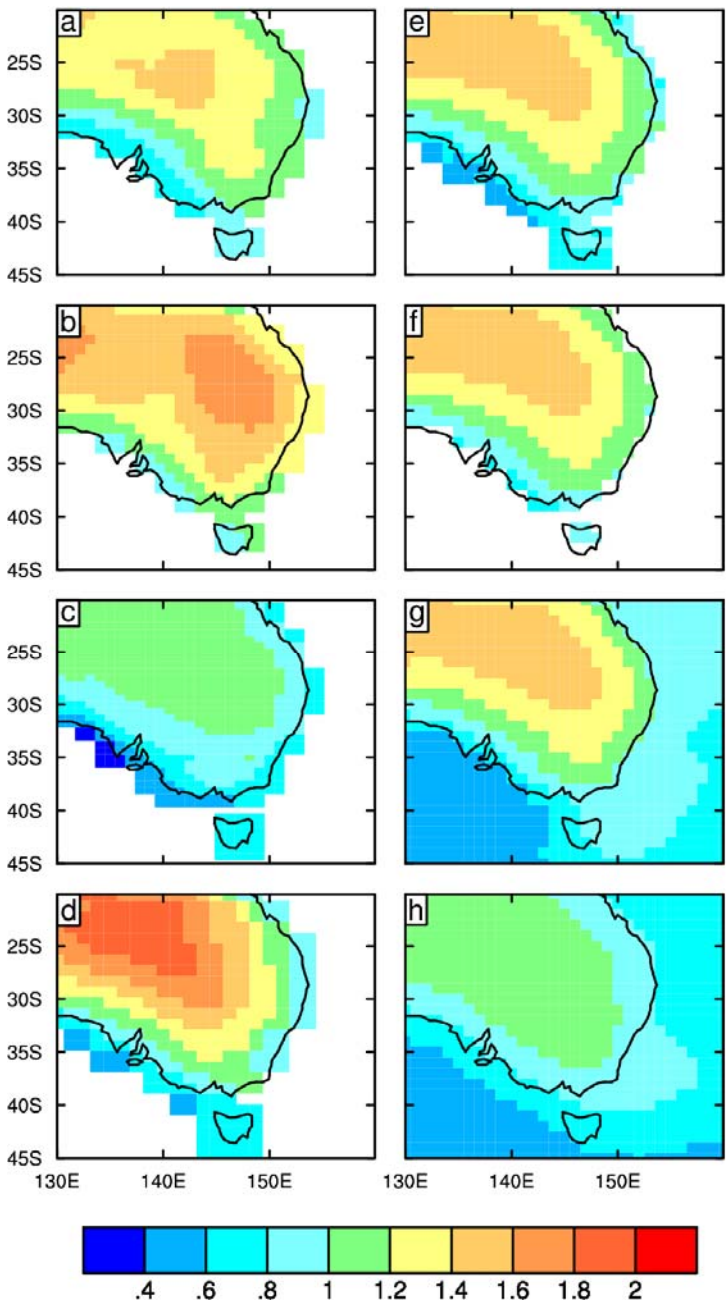

Fig. 1. Change in mean surface air temperature over SEA land divided by global annual mean change for DJF, between years 1976 and 2100, under the A1B scenario, from (a) Mk3.0, (b) Mk3.5, (c) HadGEM, (d) GFDL2.1, (e) weighted mean of one to four models, (f) weighted mean of all four models, (g) weighted mean of four models from land and sea values, and (h) AR4 multi-model mean.

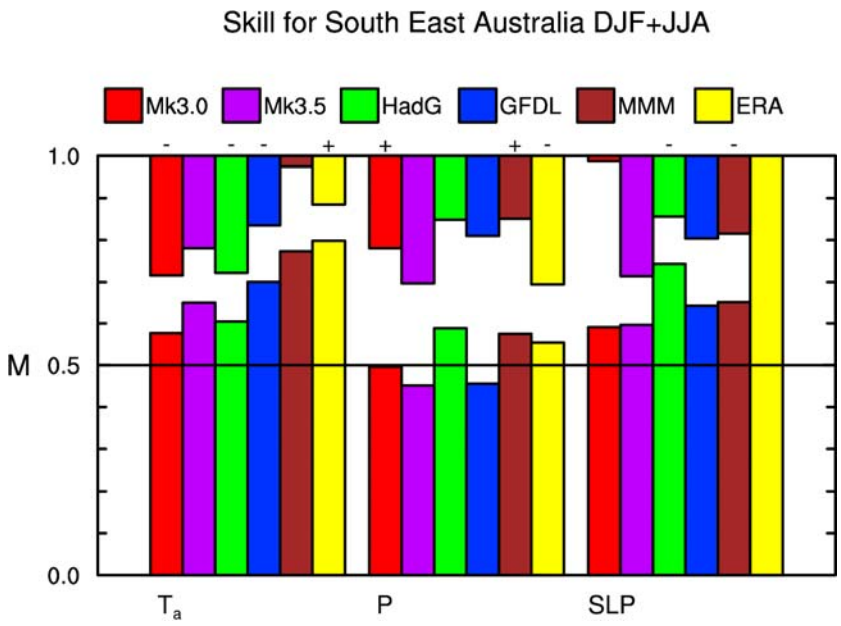

Fig. 2 Histogram representing skill of four models and the MMM in reproducing observational climatological means using data from SEA land for quantities surface air temperature (T_a), precipitation (P) and sea-level pressure (SLP). Bars up from 0 are the M score, bars down from 1 are the M score representing the mean bias over SEA. Both are averaged over the DJF and JJA results. A + or – symbol is shown when the mean bias is of the same sign in both seasons. An additional observational result from ERA40 (1958-2001) is also considered. For SLP, the M score for ERA is unity, as ERA is used as the observed. All data were interpolated to the common BOM grid, and land points in the plotted domain used.

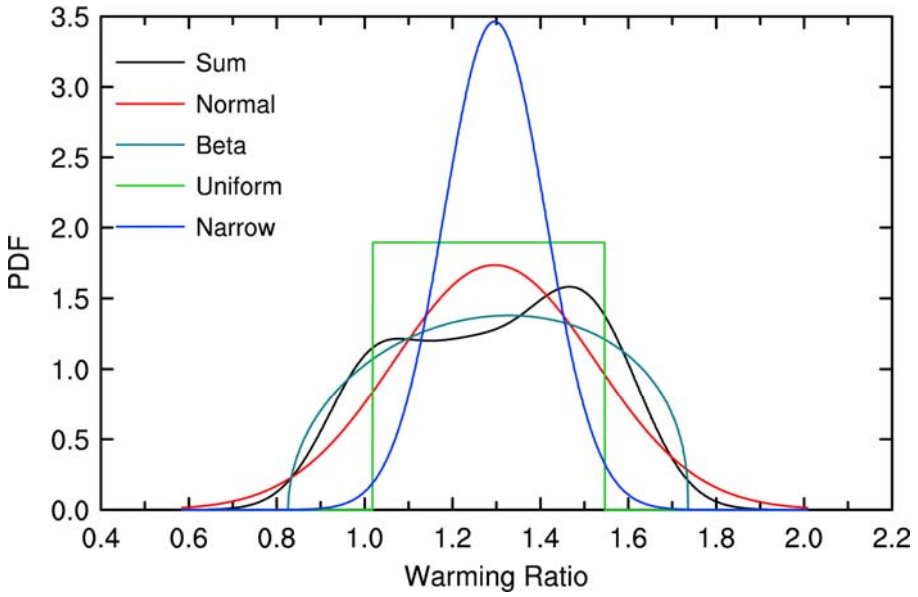

Fig. 3. Probability distribution function for the warming ratio at point 142°E, 31°S calculated from the four models, using five methods, as in key.

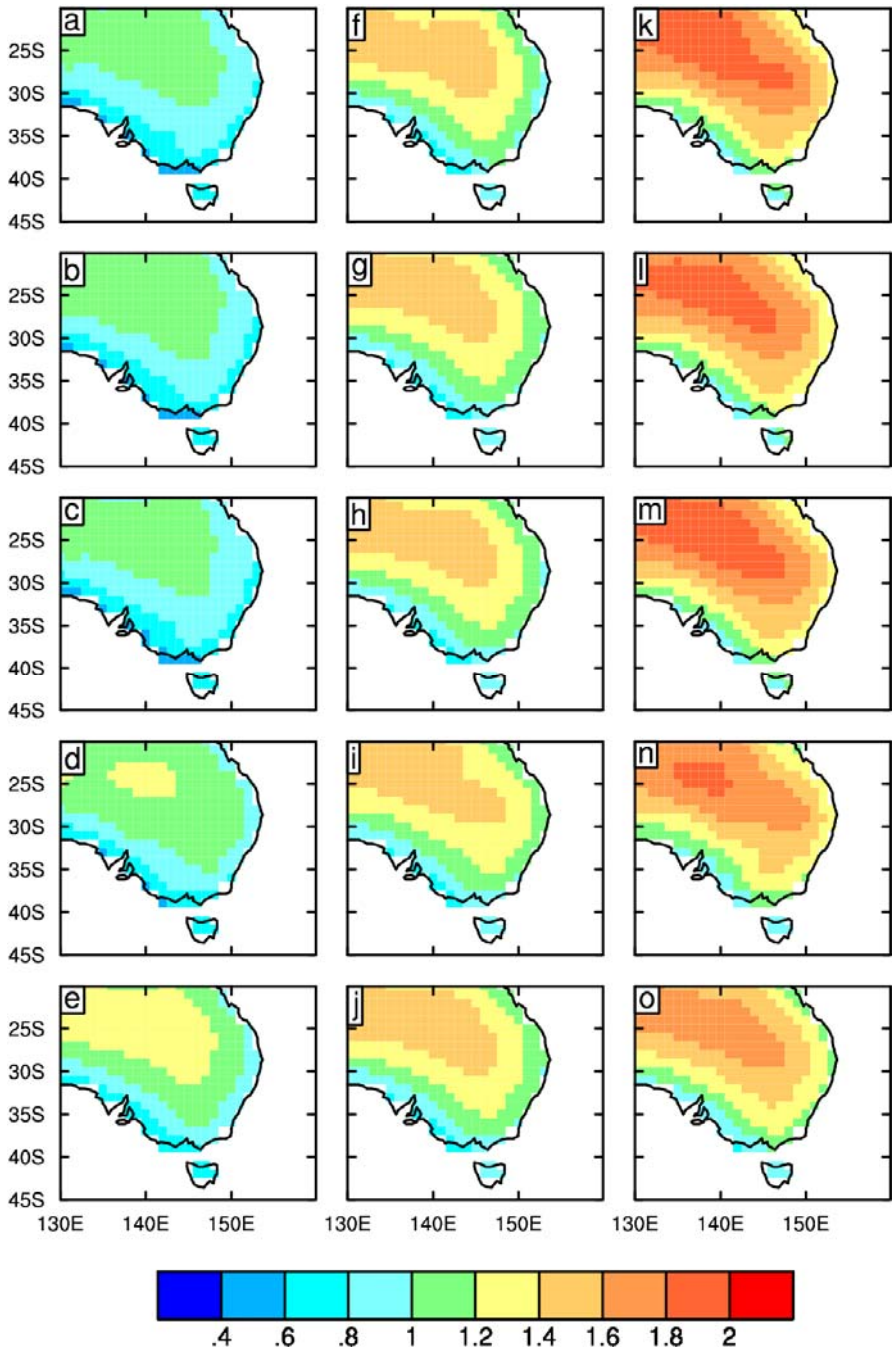

Fig. 4. Maps of percentiles of the warming ratio from all distributions (top to bottom) Sum, Normal, Beta, Uniform, and Narrow: Left column 10%, Middle column 50% and right column 90%.

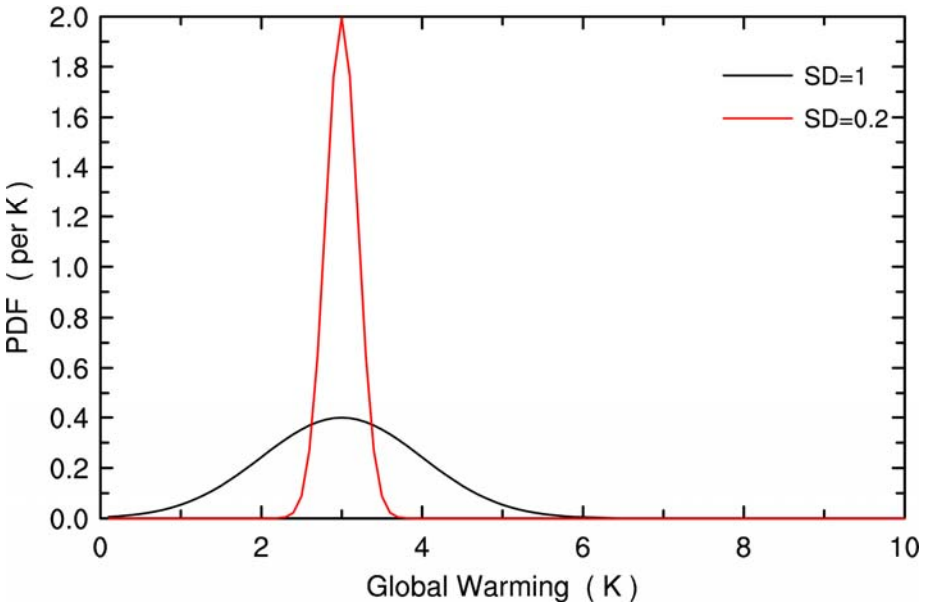

Fig. 5. Idealised distribution of global mean warming, based on the normal distribution with 3 K and SD 1 K or 0.2 K.

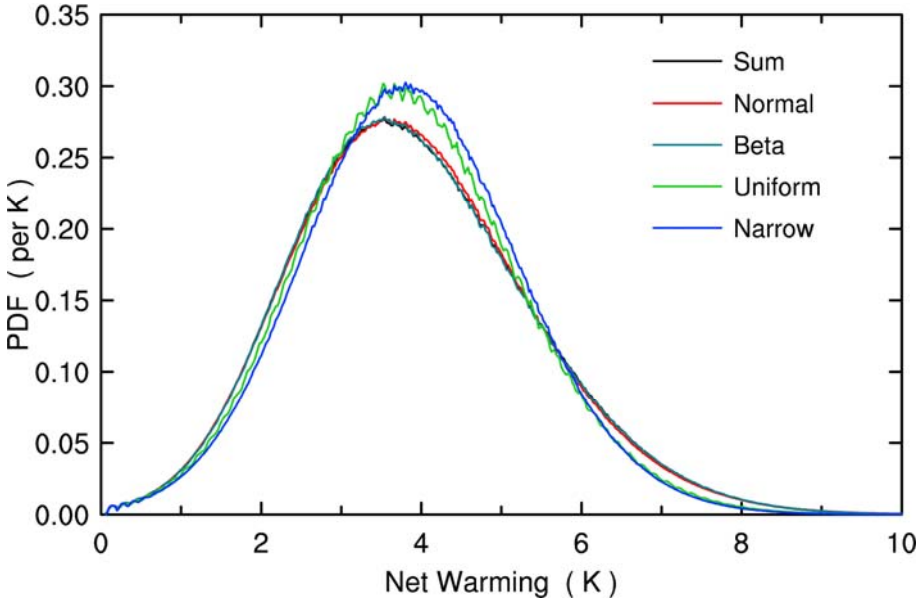

Fig. 6. Probability distribution function for net warming at point 142°E, 31°S calculated from the five ratio PDFs (as in the key) and the SD 1K global warming PDF.

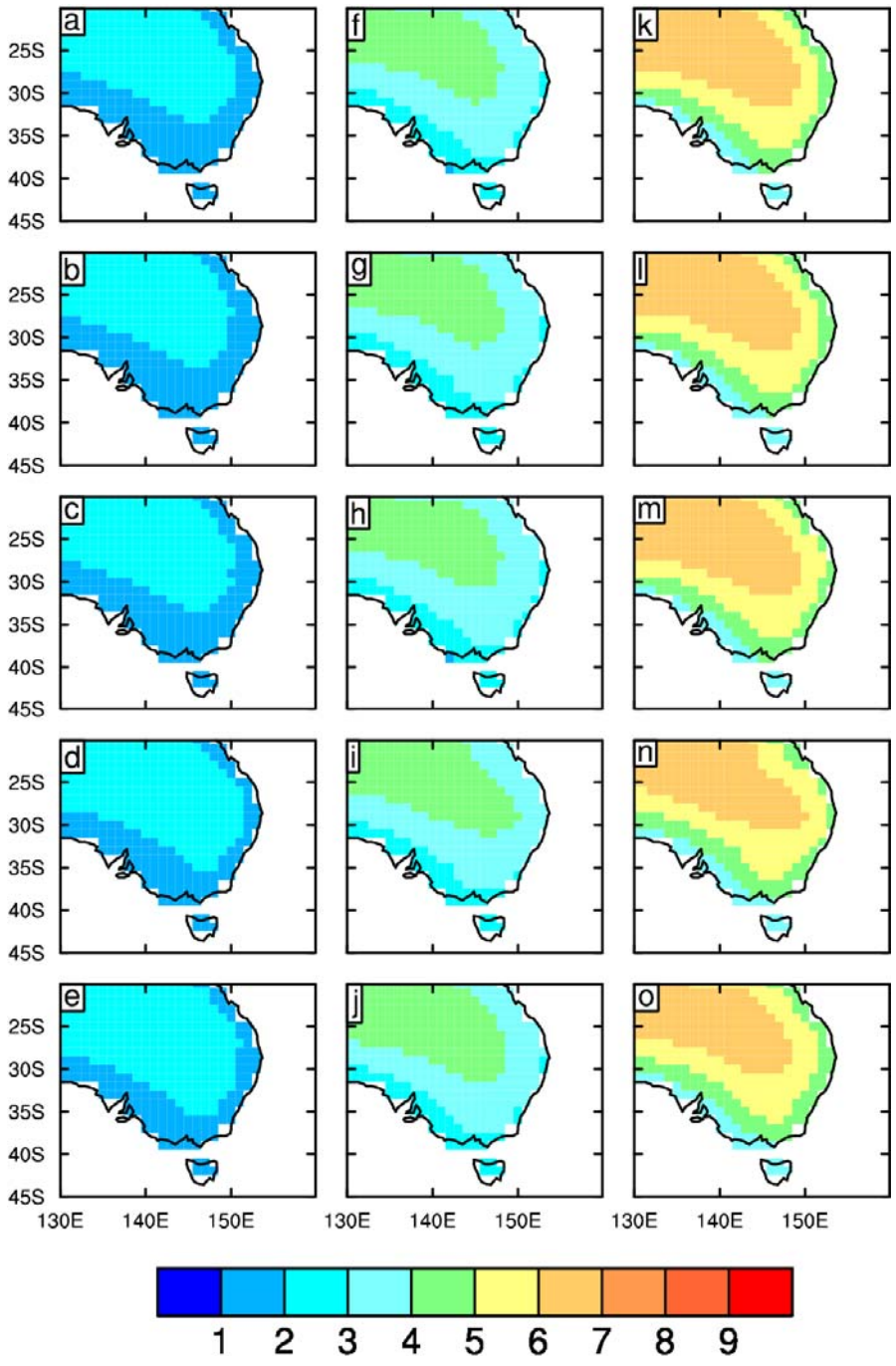

Fig. 7. Maps of percentiles of net warming from all distributions (top to bottom) Sum, Normal, Beta, Uniform, and Narrow: Left column 10%, Middle column 50% and right column 90%.

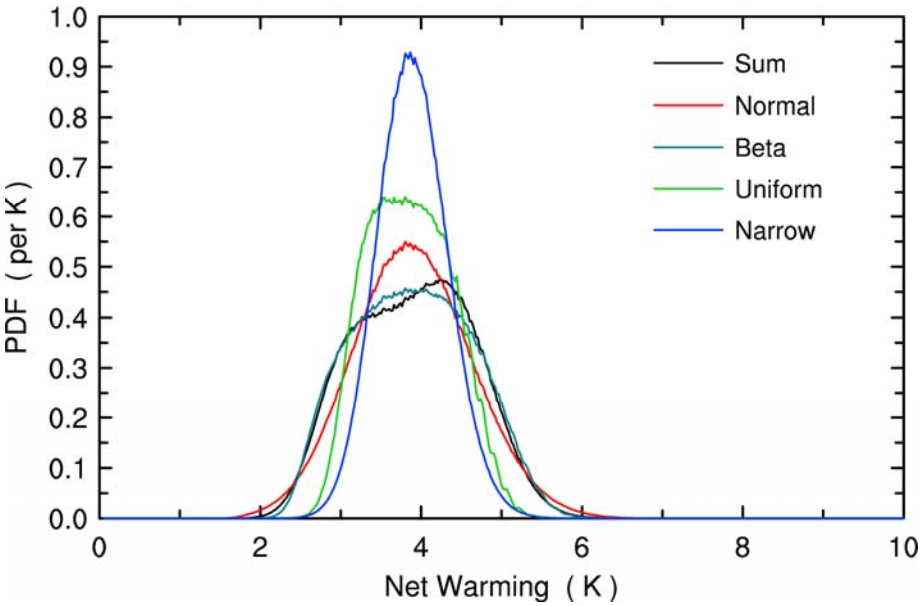

Fig. 8. Probability distribution function for the net warming at point 142°E, 31°S calculated from the five ratio PDFs (as in the key) and the SD 0.2 K global warming PDF.

References

Watterson, I. G. (2006) Some methods for specifying PDFs. *Internal report, dated 14-02-06.*

Watterson, I. G. (2005) Climate change for the IPCC scenarios simulated by the IPCC multi-model ensemble: results scaled by global mean warming. *Internal report, dated 24 May 2005.*

Watterson, I. G., J. McGregor, and K. Nguyen (2006) Influence of winds on changes in extreme temperatures near Australian coasts, as simulated by CCAM. *Abstract for the AMOS National Conference, Adelaide, February 2007*

Whetton et al. (2005) Australian climate change projections for impact assessment and policy application: A review. *CMAR Res. Papr. 1*.

For details on the CSIRO Mk3 and Mk3.5 simulations, see cherax.hpsc.csiro.au/users/dix043/mk3runs/

For the full IPCC dataset, see http://www-pcmdi.llnl.gov/ipcc/about_ipcc.php